Acta Crystallographica Section A
Foundations of Crystallography
ISSN 0108-7673

Received 14 October 2002
Accepted 4 March 2003

Solving non-periodic structures using direct methods: phasing diffuse scattering

J. C. H. Spence,[a]* J. S. Wu,[a] C. Giacovazzo,[b] B. Carrozzini,[b] G. L. Cascarano[b] and H. A. Padmore[c]

[a]Department of Physics and Astronomy, Arizona State University, Tempe, AZ 85287-1504, USA, [b]Istituto di Cristallografia, c/o Dipartimento Geomineralogico, University of Bari, Campus Universitario, Via Orabona 4, 70125 Bari, Italy, and [c]Advanced Light Source, Lawrence Berkeley Laboratory, Berkeley, CA 94729, USA. Correspondence e-mail: spence@asu.edu

The problem of reconstructing the charge density of a non-periodic sample from its diffuse X-ray scattering is considered. For a sample known to be isolated, an artificial superlattice may be assumed and the numerical direct methods of crystallography applied to the continuous distribution of diffuse scattering in order to solve the phase problem. This method is applied to simulated soft-X-ray transmission speckle patterns from a two-dimensional array of gold balls of 50 nm diameter. The results are relevant to efforts to phase the scattering from many individual macromolecules that cannot be crystallized, and to the scattering from individual inorganic nanoparticles.

1. Introduction

The high brightness of modern synchrotron sources now suggests the possibility of collecting continuous atomic resolution diffraction data from individual nanostructures, which may be poorly crystalline or not crystalline. Recent work, for example, proposed for pulsed X-ray sources is aimed at reconstructing charge densities at atomic resolution from diffraction patterns collected from successive identical macromolecules that cannot be crystallized (Neutze *et al.*, 2000; Miao *et al.*, 2001). For inorganic nanostructures, where radiation damage is less severe and continuous sources can be used, the large number of atoms present in submicrometre particles presents a severe challenge to numerical methods of phasing (Robinson *et al.*, 2001). Experimental problems in the handling and mounting of particles not visible under optical microscopes also presents difficulties. The deposition of particles from solution onto micrometre-sized silicon nitride windows has been used to address this issue (He *et al.*, 2003). A more tractable experimental project might be based on the use of a set of identical small particles, whose scattering properties are known, instead of atoms, in the direct-methods analysis. This then allows one to take advantage of the strong interaction and high spatial coherence of soft X-ray synchrotron undulator sources, which can provide sufficiently strong scattering from such small diffracting volumes.

To estimate the recording times involved, we may take a single inorganic nanoparticle consisting of about $n = 2000$ atoms (the maximum that might be phased using direct methods, as discussed below), with $Z = 80$, and use a total scattering cross section $\sigma = nZ\sigma_e$, where σ_e is the Thomson electron scattering cross section. For the proposed Energy Recovery Line (ERL) at Cornell in continuous high-coherence mode, an average brilliance of 10^{22} photons s^{-1} $(0.1\%)^{-1}$ mm^{-2} $mrad^{-1}$ is expected (Shen, 2001), giving about one count per second per pixel for a 1 K × 1 K CCD camera in the absence of background.

This paper describes a contribution to this general effort, in which we have simulated the diffuse soft-X-ray transmission diffraction pattern from a two-dimensional array of randomly positioned gold balls, whose coordinates were obtained from an experimental sample described in a companion paper (He *et al.*, 2003). 50 nm diameter balls are assumed and a 2.1 nm X-ray wavelength. We then invert this simulated diffraction pattern using direct methods to obtain the ball coordinates. The scattering factor for a single ball is calculated and replaces the atomic scattering factor normally used in direct methods.

2. Sampling and diffuse scattering

The direct-methods approach to determining the phases of structure factors is normally applied to the Bragg intensities diffracted by a crystal. Here we apply it to the diffuse scattering from a non-periodic object, in the form of an isolated cluster of gold balls. For a wavelength of $\lambda = 2.1$ nm and a single ball of diameter $d = 50$ nm, a continuous Airey-disc-like transmission pattern of scattering can be expected, with a first minimum very approximately at $\sin \varphi_0/\lambda = 1.2/d$, with φ_0 the scattering angle. For a two-dimensional cluster of balls lying on a transparent silicon nitride membrane, this pattern will be broken up into speckles owing to interference between different balls. (For two balls, the Airey disc would be crossed by Young's fringes.) We assume complete spatial and temporal coherence in the beam. Fig. 1 shows the positions of the balls assumed in this study, based on a scanning-electron-micro-

scope (SEM) image of an experimental sample prepared for a related project (Spence *et al.*, 2002; He *et al.*, 2003), in which the use of the Fienup hybrid input–output algorithm was evaluated for phasing experimental diffuse scattering from this sample. Table 1 gives the coordinates of the atoms.

If we consider a one-dimensional analysis for simplicity, in which the balls are known *a priori* to lie entirely within a domain of width W, then the Whittaker–Shannon sampling theorem guarantees that the entire continuous distribution of scattering can be reconstructed from a knowledge of its complex samples taken at spacings $n/W = \sin\varphi_n/\lambda = 2\sin\Theta_n/\lambda = \Delta S$ apart in reciprocal space (Bracewell 1965). (Sampling at half this interval would be needed to reconstruct all the diffracted intensity from samples of the intensity, since the intensity transforms to the larger autocorrelation function.) No information is lost provided this ΔS, or smaller sampling, is used while working with the complex diffracted amplitudes. These samples may therefore be treated as the 'Bragg beams' to be used in the direct-methods algorithm, with Θ_n playing the role of the Bragg angle. Evidently, a choice of camera length is required experimentally, which ensures that the pixels of the recording device sample the diffuse scattering at these sampling angles φ_n. Equally importantly, it is essential that no material outside the domain of size W contributes to the diffraction pattern, and this is the most difficult condition to satisfy experimentally. We shall refer to W as the artificial superlattice dimension. Thus we assume a square latttice with cell constant W, symmetry $P1$. The assumptions of direct methods, of non-negative charge density, of discrete non-vibrating point 'atoms' will then be applied to our non-periodic isolated cluster of gold balls (Giacovazzo, 1998). We thus assume that it is possible to make such an isolated object of approximately known size. Note that the Shannon sampling theorem does not predict that the oversampled values at $\Delta S/2$ are redundant (because they can be reconstructed from our 'Bragg' intensities recorded at intervals ΔS) – to do that, one would need the *complex* 'Bragg' amplitudes, which are not measured.

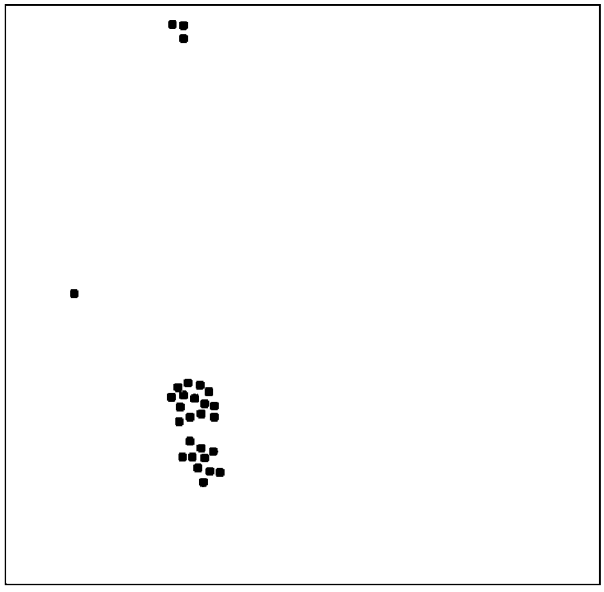

Figure 1
Positions of the 50 nm diameter gold balls assumed in this study.

Table 1
Fractional atomic coordinates (x_0, y_0) used in constructing the structure model shown in Fig. 1, based on a SEM image of a sample.

The cell constant W = 3200 nm. The lattice is square. Coordinates read from the retrieved structure solved by *SIR2002* (x_1, y_1); and coordinates (x_2, y_2) calculated from (x_1, y_1) when they have the same origin as the starting model.

Coordinates of the starting model			Coordinates of the retrieved structure			Coordinates by rotating and shifting origin to the same position	
n	x_0	y_0	n_1	x_1	y_1	x_2	y_2
1	0.3223	0.8301	Au24	0.533	0.517	0.3225	0.8293
2	0.3516	0.8125	Au25	0.504	0.535	0.3515	0.8114
3	0.3340	0.8105	Au8	0.523	0.536	0.3325	0.8103
4	0.3125	0.8047	Au10	0.542	0.541	0.3135	0.8053
5	0.3242	0.7871	Au2	0.531	0.632	0.3246	0.7143
6	0.3027	0.7852	Au16	0.551	0.561	0.3045	0.7853
7	0.2852	0.7852	Au4	0.571	0.561	0.2845	0.7853
8	0.3398	0.7754	Au11	0.515	0.571	0.3405	0.7754
9	0.3184	0.7715	Au14	0.537	0.578	0.3185	0.7683
10	0.2988	0.7578	Au27	0.557	0.587	0.2985	0.7593
11	0.3418	0.7148	Au3	0.516	0.632	0.3396	0.7144
12	0.3184	0.7090	Au15	0.536	0.635	0.3196	0.7113
13	0.2988	0.7148	Au26	0.560	0.633	0.2956	0.7133
14	0.2793	0.7227	Au18	0.577	0.625	0.2786	0.7213
15	0.3418	0.6953	Au20	0.513	0.652	0.3426	0.6944
16	0.3242	0.6914	Au7	0.531	0.656	0.3246	0.6903
17	0.2813	0.6973	Au13	0.574	0.649	0.2816	0.6973
18	0.3066	0.6816	Au23	0.549	0.666	0.3066	0.6803
19	0.2871	0.6758	Au9	0.569	0.670	0.2866	0.6763
20	0.3320	0.6699	Au28	0.523	0.674	0.3326	0.6723
21	0.3164	0.6582	Au1	0.540	0.688	0.3156	0.6583
22	0.2949	0.6543	Au6	0.560	0.692	0.2956	0.6543
23	0.2773	0.6621	Au21	0.578	0.685	0.2776	0.6613
24	0.2656	0.6797	Au12	0.588	0.667	0.2676	0.6793
25	0.0938	0.4961	Au19	0.762	0.850	0.0938	0.4961
26	0.2871	0.0449	Au17	0.569	0.302	0.2862	0.0443
27	0.2871	0.0215	Au22	0.569	0.324	0.2863	0.0223
28	0.2676	0.0195	Au5	0.588	0.327	0.2673	0.0193

3. Soft X-ray scattering factor for a single gold ball

The soft X-ray wavelengths of about 2 nm typically used for speckle research mean that the atoms of the scattering material are not resolved. The scattering distribution is related, in the Born approximation, to the Fourier transform of the refractive-index variation if absorption is negligible (Kirz *et al.*, 1995). For the small-angle scattering involved, we use a phase-object approximation to calculate the scattering factor for a single 'phase ball'. With $n = (1-\delta) - i\beta = 1 - 0.00409176 - i0.00352867$, the refractive index for gold at 588 eV (λ = 2.1 nm), a phase shift of 0.6 rad is introduced at a thickness of 50 nm of gold. Absorption is neglected. If the beam direction is z, then the thickness of a ball of radius c is

$$t(\mathbf{r}) = 2(c^2 - r^2)^{-1/2}, \qquad (1)$$

where $\mathbf{r}$ is a two-dimensional vector normal to the beam. Then the phase change is $\theta(\mathbf{r}) = 2\pi t(\mathbf{r})\delta/\lambda$ and depends on the thickness and refractive index of the materials. The real part of the refractive index is $\delta = (r_e\lambda^2/2\pi)n_a f$, with n_a atoms per unit

Table 2
List of the scattering factors of the 'phase ball': their assigned index h, k and scattering vector **s**, moduli $|\mathbf{F}|$ and phase (φ) of the scattering factor.

h	k	**s** (Å^{-1})	$\lvert\mathbf{F}\rvert$	Phase (φ) (°)
0	0	0	49.8299	1.38741
0	3	0.00009375	49.6775	−2.17654
0	4	0.000125	49.5592	0.824723
0	5	0.00015625	49.4075	−2.45697
0	6	0.0001875	49.2225	0.544761
0	7	0.00021875	49.0044	−2.73646
0	8	0.00025	48.7538	0.265744
0	11	0.00034375	47.810	2.99065
0	14	0.0004375	46.589	−0.565288
0	15	0.00046875	46.1232	2.43874
0	20	0.000625	43.3862	−1.38611
0	25	0.00078125	40.0510	1.081
0	28	0.000875	37.8164	−2.46018
0	33	0.00103125	33.8077	0.0260841
0	38	0.0011875	29.5924	2.52952
0	44	0.001375	24.5350	1.79556
0	47	0.00146875	22.1174	−1.69539
0	48	0.0015	21.3410	1.33297
0	55	0.00171875	16.5398	−2.5462
0	58	0.0018125	14.9435	0.312414
0	63	0.00196875	13.0830	3.02169
0	66	0.0020625	12.4702	−0.366913
0	71	0.00221875	12.1641	2.35148
0	78	0.0024375	12.5733	−1.45913
0	87	0.00271875	13.0460	0.685628
0	102	0.0031875	11.2654	1.98972
0	119	0.00371875	5.6846	3.08236
0	138	0.0043125	3.0356	−0.706303
0	149	0.00465625	5.33447	1.33431
0	158	0.0049375	6.21723	−2.95001
0	167	0.00521875	5.93688	−1.00205
0	188	0.005875	1.81899	−0.596501
0	211	0.00659375	3.56755	2.18732
0	228	0.007125	4.57765	2.98487
0	233	0.00728125	4.23598	−0.855169
0	248	0.00775	1.8013	0.18083
0	251	0.00784375	1.14399	2.89991

volume, r_e the classical electron radius and f the atomic scattering factor for one Au atom. Away from absorption edges, the charge density is related to δ by $\rho(\mathbf{r}) = (2\pi/r_e\lambda^2)\delta(\mathbf{r})$.

If the iconal approximation is made, such that the wavefield across the downstream face of the two-dimensional array of balls can be computed along a single optical path through the balls, then a transmission function, giving the ratio of the exit-face wavefield to the incident wavefield can be defined as

$$q(\mathbf{r}) = \exp[2\pi i t(\mathbf{r})\delta/\lambda] = \exp[i\theta(\mathbf{r})]. \quad (2)$$

This assumes that Fresnel broadening of the wavefield is negligible within the ball, and so is equivalent to the assumption of a planar Ewald sphere. This is a good approximation if $t_{\max} < d^2/\lambda$, for spatial frequency (resolution) d and a maximum ball thickness $t_{\max}$. The approximation thus fails for hard X-rays at atomic resolution, but is reasonable for 50 nm diameter balls at $\lambda = 2.5$ nm out to a resolution of about 10 nm. The scattering factor of one gold ball is the two-dimensional Fourier transform of the transmission function:

$$f^{\text{ball}}(\mathbf{u}) = \int_{\Omega} q(\mathbf{r}) \exp(-2\pi i \mathbf{u}\cdot\mathbf{r})\, \mathrm{d}\Omega, \quad (3)$$

where $u = \sin\varphi/\lambda$. It is convenient to use $\mathbf{r}$–θ coordinates in the integration since the function is radially symmetric:

$$f^{\text{ball}}(\mathbf{u}) = \int_0^c \mathbf{r} \exp\{[4\pi i\delta(c^2 - r^2)^{1/2}]/\lambda\}\, \mathrm{d}r \times \int_0^{2\pi} \exp(-2\pi i \mathbf{u}\cdot\mathbf{r}\cos\Theta)\, \mathrm{d}\Theta,$$

where Θ is the angle between **u** and **r**. In terms of the zero-order Bessel function

$$J_0(z) = (1/2\pi)\int_0^{2\pi} \exp(-iz\cos\Theta)\, \mathrm{d}\Theta,$$

we have:

$$f^{\text{ball}}(\mathbf{u}) = 2\pi \int_0^c \mathbf{r} \exp\{[4\pi i\delta(c^2 - r^2)^{1/2}]/\lambda\} J_0(2\pi\mathbf{u}\cdot\mathbf{r})\, \mathrm{d}r. \quad (4)$$

This two-dimensional Fourier transform of a circularly symmetric function is a Hankel transform of order zero. This may be written in terms of sums over certain generalized hypergeometric functions and γ functions, or expanded in other ways. The integral can also be solved by numerical integration. The calculated scattering factors of the 'phase ball' are complex, which implies that the scattering phases are not zero, as in the usual kinematic approximation.

We now consider whether Friedel's law holds for these complex scattering factors. Since the zero-order Bessel function is an even function $f(\mathbf{u}) = f(-\mathbf{u}) = |f|\exp(i\alpha)$, the structure factors for **u** and −**u** are:

$$F(\mathbf{u}) = \sum_i f_i(\mathbf{u}) \exp(i\alpha) \exp(2\pi i \mathbf{u}\cdot\mathbf{r}_i)$$

$$F(-\mathbf{u}) = \sum_i f_i(\mathbf{u}) \exp(i\alpha) \exp(-2\pi i \mathbf{u}\cdot\mathbf{r}_i).$$

The complex conjugate of $F(\mathbf{u})$ is:

$$F^*(\mathbf{u}) = \sum_i f_i(\mathbf{u}) \exp(-i\alpha) \exp(-2\pi i \mathbf{u}\cdot\mathbf{r}_i).$$

$F(-\mathbf{u})$ is no longer the complex conjugate of $F(\mathbf{u})$. However, since all the balls are assumed to scatter equally, the scattering amplitudes remain equal, but phases no longer reverse sign under inversion. For a general function $t(\mathbf{r})$ in this iconal approximation, such as would result from many different balls, Friedel's law does not apply to the scattering. We assume identical balls, and hence that Friedel's law, which requires $I_u = I_{-u}$, will apply for these complex scattering factors. For smaller balls, such that $\theta < \pi/2$, we have $\exp[i\theta(\mathbf{r})] \simeq 1 + i\theta(\mathbf{r})$, then the Fourier transform becomes

$$\begin{aligned}\Im[1 + i\theta(\mathbf{r})] &= 2\pi \int_0^c \mathbf{r}\{[1 + i4\pi\delta(c^2 - r^2)^{1/2}]/\lambda\} J_0(2\pi\mathbf{u}\cdot\mathbf{r})\, \mathrm{d}r \\ &= 2\pi \int_0^c \mathbf{r} J_0(2\pi\mathbf{u}\cdot\mathbf{r})\, \mathrm{d}r \\ &\quad + i(8\pi^2\delta/\lambda) \int_0^c \mathbf{r}(c^2 - r^2)^{1/2} J_0(2\pi\mathbf{u}\cdot\mathbf{r})\, \mathrm{d}r, \end{aligned} \quad (5)$$

in which the first term represents the undiffracted beam and the second term, which is the Fourier transform of $\theta(\mathbf{r})$, is equal to the scattering factor of a gold ball in the kinematic

approximation. Since the scattering factor of one ball is now real for a weak phase object, Friedel's law will then hold also for weakly scattering balls (even if not identical) and, in addition, $F(\mathbf{u}) = F^{*}(-\mathbf{u})$.

4. Direct methods applied to an artificial superlattice

Fig. 1 shows the structural model of the phase 'balls'. Each ball has a diameter of 8 pixels and the whole image is 512×512 pixels. Since the diameter of each ball is 50 nm, the resulting computational square supercell has dimension $W = 3200$ nm. The diffraction pattern also has dimension 512×512 with largest index 256. The first pixel beside the origin of reciprocal space corresponds to $1/3200\ \mathrm{nm}^{-1}$, and the maximum data resolution is then 8.84 nm, about 17.7% of the diameter of the gold ball. We have assumed $\lambda = 2.1$ nm, hence the scattering angle for the first pixel is $\theta = \lambda/d = 2.1/3200 = 0.00066$ rad. Using a pixel size of $d_p = 24\ \mu$m, the object–detector distance L in our simulation becomes $L = d_p/\theta = 36.6$ mm.

The simulated diffraction pattern is shown in Fig. 2: this is the continuous distribution of scattering, then it is sampled at intervals $u_n = nW$. In practice, we treat the intensity in the first pixel besides the center as if it were a first-order Bragg beam. The space group was set as $P1$. A one-dimensional representation of the scattering factor (both the amplitudes and phases) for one 'phase ball' is shown in Fig. 3(*a*). The modulus of the Fourier transform of a single phase ball is shown in Fig. 3(*b*). The limited number of pixels per ball accounts for the lack of circular symmetry. The variation of the amplitude and phase for one phase ball's scattering factor with scattering vector **u** is given in Table 2.

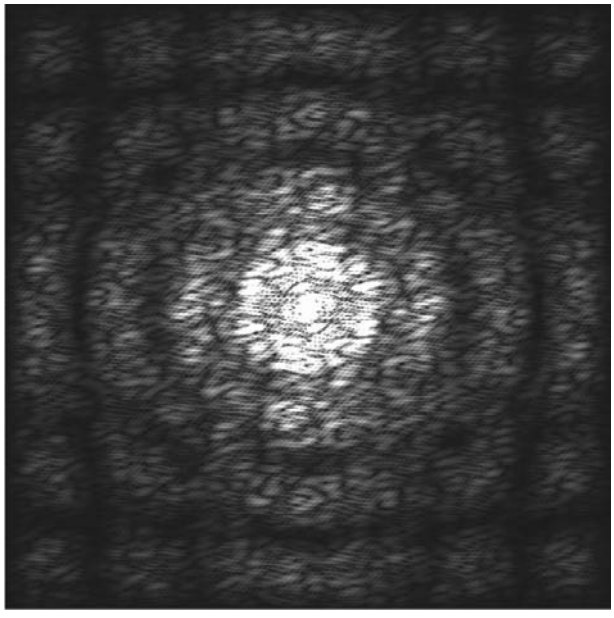

Figure 2
Simulated speckle pattern by Fourier transform of the gold balls shown in Fig. 1 and assuming each ball as a 'phase ball'.

To apply direct methods, we first normalize structure factors according to

$$E_{\mathbf{h}} = \sum_j f_j(\mathbf{h}) \exp(2\pi i \mathbf{h} \cdot \mathbf{r}_j) \Big/ \Big[\sum_j f_j(\mathbf{h}) 2 \Big]^{1/2}. \qquad (6)$$

Assuming that all balls are identical, (6) reduces to

$$E_{\mathbf{h}} = N^{-1/2} \sum_j \exp(2\pi i \mathbf{h} \cdot \mathbf{r}_j). \qquad (7)$$

To obtain the normalized structure factors (7), we have divided the calculated speckle pattern by another speckle pattern which is the Fourier transform of a single ball (Fig. 3*b*). Then the normalized intensities $|E_h|^2$ of each beam were read from the resulting pattern: in this situation, the normalized scattering of the ball is considered a constant, equal to $N^{-1/2}$, independent of scattering angle. The pattern obtained when Fig. 2 is divided by Fig. 3(*b*) is shown in Fig. 4.

We now treat the sampled values of the diffuse scattering as Bragg beams by a direct-methods procedure. We used the *SIR2002* (Burla *et al.*, 2002) program to determine the positions of the gold balls. An advantage of the program is that it can handle two-dimensional intensity data: in addition, it was properly modified to handle very high two-dimensional indices (up to 512).

The tangent procedure is started from random phases: the various trial solutions are then processed by a real-space refinement including the following steps:

(*a*) *EDM*, an electron-density-modification procedure, consisting of 2 supercycles, each constituted by 5 microcycles $\rho \rightarrow \{\varphi\} \rightarrow \rho$. The symbol ρ represents the electron-density map, calculated by using all the measured scattering amplitudes, the phases are evaluated through the map inversion.

(*b*) *HAFR*, constituted by 6 cycles $\rho \rightarrow \{\varphi\} \rightarrow \rho$. In this step, the calculated structure factor is obtained by associating the normalized scattering factor of the ball ($N^{-1/2}$) with the selected peaks in the electron density map.

(*c*) *FR*, a *Fourier recycling* routine (6 cycles), which optimizes the isotropic displacement parameter for all 'atoms'.

(*d*) *DLSQ*, a procedure that alternates least squares and $(2F_{\mathrm{obs}} - F_{\mathrm{cal}})$ map calculations to refine and complete the structural model.

The quality of the trial solutions is checked at the end of the phasing process *via* the crystallographic residual

$$\mathrm{RES} = \sum ||F_{\mathrm{obs}}| - F_{\mathrm{calc}}|| / \sum |F_{\mathrm{obs}}|.$$

As seen in Table 1, *SIR2002* easily recovers all the positions of the gold balls: the process ends with a RES value of 0.0026.

In a real experiment, part of the diffraction pattern is lost owing to a beam stop blocking the direct beam. The hybrid input–output algorithm (*HiO*; Fienup, 1982) proved to be rather sensitive (Miao *et al.*, 2001) to the presence of the data in the central patch when using experimental data rather than simulated data. To check the sensitivity of the *SIR2002* algorithm, we omitted from the procedure all the data contained in a 50 pixel radius circular area at the center of the pattern, much larger than the region

typically obscured by a beam stop. All the ball positions were recovered, with the same RES value.

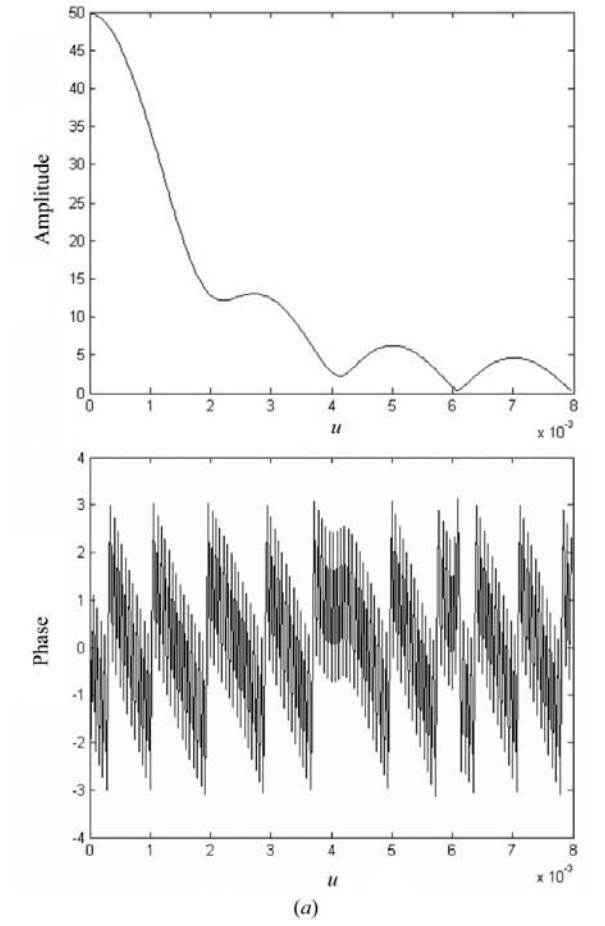

(*a*)

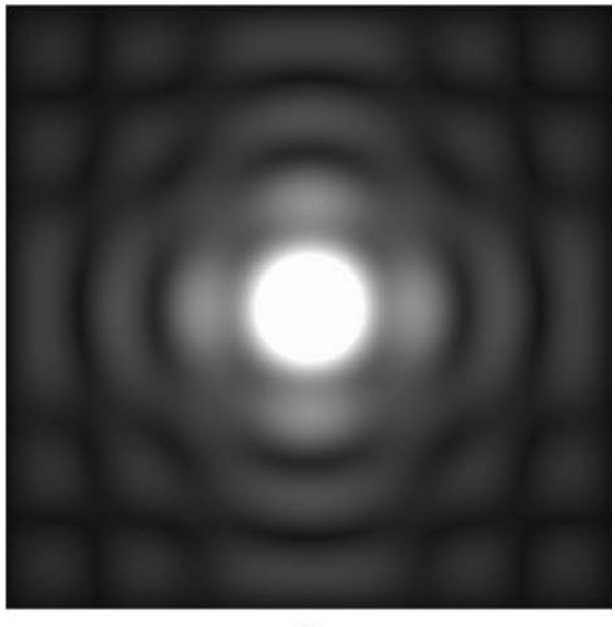

(*b*)

Figure 3
(*a*). The amplitudes and phases of the calculated scattering factors of the 'phase ball'. Note that the phases are not constant as for kinematic scattering. (*b*) Fourier transform of a single 'phase ball'.

We now consider the relationship between the *HiO* and the *SIR2002* algorithm. According to the *HiO* oversampling method (Miao *et al.*, 2001), sampling a diffraction pattern more finely than a Nyquist or 'Bragg' sampling frequency is equivalent to surrounding the electron density of the scattering object by a region of zero scattering density. Sampling at twice the Bragg frequency extracts sufficient information from the diffracted intensity to solve the phase problem using iterative algorithms (Fienup, 1982; Spence *et al.*, 2002). Progressively zeroing or depleting the zero-density area is the basis of the *HiO* algorithm, and so is akin to density-modification methods in crystallography. The use of direct methods applied to samples of diffuse scattering taken at half the 'Bragg' angle (with corresponding application of a zero-density region outside the object boundary) may therefore have advantages. The *SIR2002* algorithm does not explicitly use this information: the convergence of the phasing process is obtained by inverting up to about 3.5% of the electron density, no matter where (in the unit cell) it is. This ensures convergence even when the phases provided by the tangent formula are found relative to an origin different from that assumed by the *HiO* algorithm. So far, despite impressive simulations, we have not been successful in combining the *HiO* and direct-methods approaches in application to experimental data.

Fig. 5(*a*) shows a charge-density map of the balls based on these coordinates, and this is compared in Fig. 5(*b*) with a SEM image of the object.

5. Discussion and conclusions

We have shown that the direct-methods (DM) approach may be extended to non-periodic objects, and so used to phase

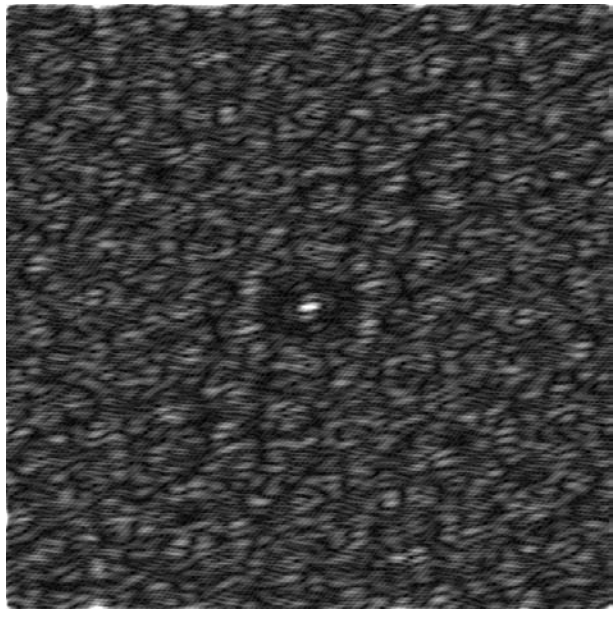

Figure 4
Calculated speckle pattern using the complex amplitudes in Fig. 2 divided by Fig. 3(*b*). The scattering factor of a gold ball can then be treated as constant using the resulting set of data.

diffuse scattering from an isolated object. In a companion paper (He *et al.*, 2003), we describe experimental work in which images of these same balls are recovered using the hybrid input–output iterative algorithm, together with a knowledge of the cluster outlines.

Our use of soft X-rays was indicated by their high coherence and strong interaction (needed to obtain sufficient signal from such a small scattering volume), and the use of gold balls instead of atoms then follows from the wavelength limit on resolution and the limited number of 'atoms' that can be handled using direct methods.

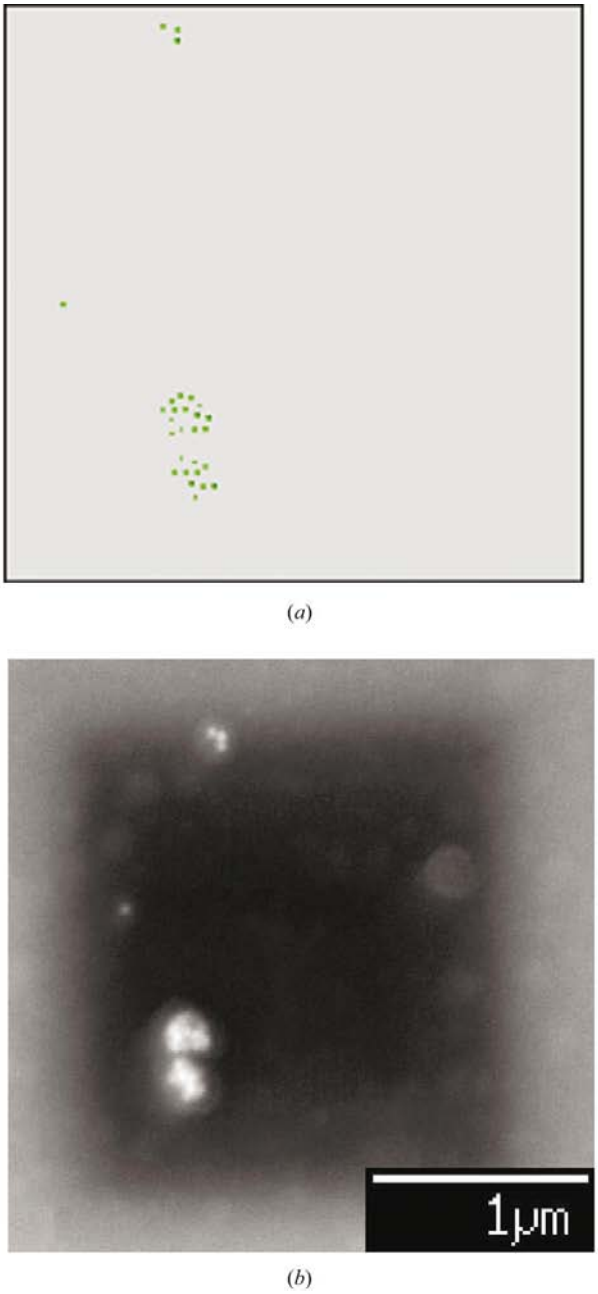

Figure 5
(*a*) Map of the reconstructed structure as obtained by direct methods. (*b*) Experimental SEM image of the same gold balls for comparison. The dark square is the window, from within which the ball positions were extracted. Balls are also seen outside the window, on the partially transparent silicon support.

Any experimental implementation of this approach must consider carefully the following. Friedel's law is assumed in the DM algorithm we used. Departures from it in experimental data might be expected owing to several factors: (i) Absorption effects may be small within a silicon nitride supporting window, but may be larger for balls lying on partially transparent material surrounding the window. (ii) The occurrence of phase shifts larger than $\pi/2$ in (2). For example, phase shifts introduced across the silicon border surrounding a silicon nitride window would differ at each ball, rendering them inequivalent and hence leading to failure of Friedel symmetry. (iii) Strains in the sample may cause a failure of Friedel's law. This might arise from icosahedral misfit in the gold spheres. (iv) The illuminating wavefront must be planar. Large phase shifts impressed across the object by the illumination would make the balls inequivalent phase objects, with large phase differences. We note that a statistical variation in the size of the balls will not violate Friedel symmetry provided the phase shift across the balls is small. (In our case the phase shift is 0.6 rad.)

The formation of an isolated object containing a sufficiently small number of atoms presents serious experimental problems, however several schemes have been proposed to achieve this, using, for example, macromolecules injected into vacuum across a pulsed beam (Neutze *et al.*, 2000). The use of DM is restricted to atomic resolution data and to nanostructures containing fewer than about 2000 atoms, with about seven strong 'beams' (detector pixels) per atom. However, the ability to determine some phases for larger structures could prove very powerful, since *a knowledge of phase is a convex constraint* (He *et al.*, 2002). It can therefore be expected to improve greatly the convergence of iterative phasing schemes based on the Fienup–Gerchberg–Saxton algorithm (Fienup, 1982; Elser, 2003), which has much in common with the electron-density-modification approach used in crystallography (Spence *et al.*, 2002). A powerful approach to larger nanostructures when atomic resolution data is used with coherent hard X-rays may therefore combine features of both the direct-methods approach and the iterative algorithms. One may use, for example, a support or object mask consisting of the autocorrelation function of the object in combination with DM. The object density is set to zero outside the masked regions. In this way, improved reconstructions might be obtained that require a less detailed knowledge of the sample's external shape, and that are more tolerant to the loss of the low spatial frequencies obscured by the beam stop.

This work was supported by ARO award DAAD190010500 and by the Director, Office of Energy Research, Office of Basic Energy Sciences, Materials Sciences Division of the US Department of Energy, under contract No. DE-AC03-76SF00098. We are grateful to Drs S. Marchesini, H. He and M. Howells for many stimulating conversations.

References

Bracewell, R. (1965). *The Fourier Transform and its Applications*. New York: McGraw-Hill.

Burla, M. C., Carrozzini, B., Cascarano, G. L., Giacovazzo, C. & Polidori, G. (2002). *Z. Kristallogr.* **217**, 629–635.

Elser, V. (2003). *J. Opt. Soc. Am.* A**20**, 40–55.

Fienup, J. R. (1982). *Appl. Opt.* **21**, 2758–2769.

Giacovazzo, C. (1998). *Direct Phasing in Crystallography*. IUCr/Oxford University Press.

He, H., Howells, M., Marchesini, S., Spence, J., Weierstall, U., Wu, J. & Giacovazzo, C. (2002). X-ray Microscopy 2002, Grenoble, France.

He, H., Marchesini, S., Howells, M., Weierstall, U., Hembree, G. & Spence, J. C. H. (2003). *Acta Cryst.* A**59**, 143–152.

Kirz, J., Jacobsen, C. & Howells, M. (1995). *Q. Rev. Biophys.* **28**, 33–130.

Miao, J., Hodgson, K. O. & Sayre, D. (2001). *Proc. Natl Acad. Sci. USA*, **98**, 6641–6645.

Neutze, R., Wouts, R., van der Spoel, D., Weckert, E. & Hajdu, J. (2000). *Nature (London)*, **406**, 752–757.

Robinson, I. K., Vartanyants, I. A., Williams, G. J., Pfeifer, M. A. & Pitney, J. A. (2001). *Phys Rev Lett*. **87**, 195505.

Shen, Q. (2001). *CHESS Tech. Memo*, 01–003.

Spence, J., Weierstall, U. & Howells, M. (2002). *Philos Trans.* **360**, 1–21.